

Estimating linear mass transport coefficients in solid solutions via correlation splitting and a law of total diffusion

Manuel Athenes, Gilles Adjanor, Jérôme Creuze

▶ **To cite this version:**

Manuel Athenes, Gilles Adjanor, Jérôme Creuze. Estimating linear mass transport coefficients in solid solutions via correlation splitting and a law of total diffusion. Physical Review Materials, 2022, 6, pp.013805. 10.1103/PhysRevMaterials.6.013805 . cea-03745969

HAL Id: cea-03745969
https://cea.hal.science/cea-03745969

Submitted on 4 Aug 2022

HAL is a multi-disciplinary open access archive for the deposit and dissemination of scientific research documents, whether they are published or not. The documents may come from teaching and research institutions in France or abroad, or from public or private research centers.

L'archive ouverte pluridisciplinaire **HAL**, est destinée au dépôt et à la diffusion de documents scientifiques de niveau recherche, publiés ou non, émanant des établissements d'enseignement et de recherche français ou étrangers, des laboratoires publics ou privés.

Estimating linear mass transport coefficients in solid solutions via correlation splitting and a law of total diffusion

Manuel Athènes,[1] Gilles Adjanor,[2] and Jérôme Creuze[3]
[1]*Université Paris-Saclay, CEA, Service de Recherches de Métallurgie Physique, F-91191 Gif-sur-Yvette, France*
[2]*EDF Lab les Renardières, Département Matériaux et Mécaniques des Composants, F-77818 Moret-sur-Loing, France*
[3]*Université Paris-Saclay, ICMMO, CNRS UMR 8182, F-91405 Orsay Cedex, France*

(Received 1 June 2021; accepted 3 January 2022; published 27 January 2022)

Directly computing linear mass transport coefficients in stochastic models entails integrating over time the equilibrium correlations between atomic displacements. Here, we show how to improve the accuracy of kinetic Monte Carlo simulations via correlation splitting and conditioning, which statistically amounts to estimating the mass transport coefficients through a law of total diffusion. We illustrate the approach with kinetic path sampling simulations of atomic diffusion in a random alloy model in which percolating solute clusters trap the mediating vacancy. There, Green functions serve to generate first-passage paths escaping the traps and to propagate the long-time dynamics. When they also serve to estimate mean-squared displacements via conditioning, colossal reductions of statistical errors are achieved.

DOI: 10.1103/PhysRevMaterials.6.013805

I. INTRODUCTION

Mass transport is the natural phenomenon that governs both the time evolution of thermodynamic systems towards equilibrium and the diffusion of chemical species at equilibrium. Its understanding is fundamentally important and challenging in many engineering applications, ranging from biophysics to materials science. Equilibrium correlations between particle displacements play a crucial role because they allow characterizing transport coefficients close to equilibrium owing to linear response theory [1,2]. Hence, chemical currents in solid solutions can be expressed as products of diffusion matrices and negative gradients of chemical concentrations considered as small thermodynamic forces. In crystalline solids, atomic transport is mediated by defects [3,4], most often by vacancies exchanging with neighboring substitutional atoms. Interstitial atoms jumping to adjacent interstitial sites also contribute to atomic diffusion, in irradiated alloys especially [5,6]. Usually, atomic hops are thermally activated processes occurring at rates that are well predicted by transition state theory and its extensions [7]. There, states correspond to local minima of the potential energy surface. They span a discrete space embedded into the continuous space which the dynamical system evolves in. Transition rates computed at the atomic scale possibly include anharmonic [8], quantum [9], and dynamical [10] corrections, whose respective contributions depend on temperature T. Dynamical corrections are to be included to account for memory effects when state-to-state transitions depend on past transitions [10]. They may be significant in simulations of dynamical systems evolving on complicated potential energy surfaces over long timescales when the encountered barrier heights ΔE are similar or lower than the thermal energy k_BT (k_B stands for Boltzmann's constant). This specific situation occurs, for example, at moderately high temperatures in pure α-iron, where the activation energies for the migration of glissile clusters of self-interstitial atoms may be particularly small, on the order of tens of meV [11,12]. When the imposed temperature is low enough, the atomic dynamics in the basin of attraction of every visited state reaches a local quasistationary distribution prior to transitioning to another state and the system becomes memoryless [13]. This entails that the transition rates do not depend any more on which transition occurred previously. Such transitions are said to be Markovian. In solid solution alloys and compounds, the temperatures of interest are usually low enough so that transitions be considered Markovian. Atomic scale modeling of mass transport then relies on the ability to evaluate an exhaustive list of the important elementary transition rates [14]. This makes it possible to construct realistic discrete-space models satisfying the Markov property. Such a description does not preclude complex transport mechanisms to involve concerted atomic displacements [15]. Generic models based on master equations are also very useful as they allow investigating the interplay between transition rates and transport properties by varying their physical parameters in a systematic manner [3].

Kinetic Monte Carlo (kMC) [16,17] provides a direct method to estimate transport coefficients in physical systems governed by high-dimensional master equations. However, the method is hindered by the low occurrence of important events. A considerable amount of computations are often needed to collect sufficient statistics in many systems of interest [18,19], including basic models of defect migration through homogeneous media [15]. Besides, low-complexity models are amenable to nonstochastic master-equation approaches [20–23] that may yield accurate predictions at much lower cost. These methods involve integrating fundamental matrices [20,22,24] or equivalently evaluating lattice Green

 ©2022 American Physical Society

functions [25,26] that either minimize a variational problem [27–29] or satisfy a Poisson equation [30–33]. The dimension of the linear systems to solve and the viability of approximations made to handle exponentially increasing numbers of configurations limit the applicability of nonstochastic approaches.

Here, we develop a correlation splitting and conditioning scheme aiming to facilitating the estimation of linear mass transport coefficients at thermodynamic equilibrium using conventional and advanced kinetic Monte Carlo simulations. The approach alleviates the aforementioned issues: scarcity of harvested important events and combinatorial explosion in numerical algebra. It furthermore leads us to formulate a law of total diffusion (LTD) that relates to the laws of total expectation (LTE) and variance (LTV) considered so far to compute thermodynamic expectations and their statistical variance via conditioning [32–41]. We illustrate the approach on a random alloy model [29] exhibiting dynamical trapping and percolation by estimating the diffusion matrix, denoted below by $\mathbb{D}[\mathbf{d}]$ and defined as half the asymptotic variance of the vector $\mathbf{d}$ of chemical displacements.

II. DIFFUSION MATRIX FOR REVERSIBLE MARKOV CHAINS

To monitor the displacements of each of the c chemical species along each of the s space dimensions, any state χ is mapped onto a descriptor $\mathbf{r} \in \mathbb{R}^{sc}$. Component r_i represents here the coordinate sum of all α-type atoms in space direction a, the descriptor index being encoded as $i = a + s(\alpha - 1)$, where $a \in \mathbb{N}_s^\star$ and $\alpha \in \mathbb{N}_c^\star$. Then, displacement $\mathbf{d}(\chi, \chi')$ from state χ to state χ' is computed using the minimum image representation of $\mathbf{r}' - \mathbf{r}$.[1] The variance matrix of vector $\mathbf{r}$ over a Markov chain reads as $\mathbb{V}[\mathbf{r}] = \mathbb{E}[\mathbf{r}^2] - \mathbb{E}[\mathbf{r}]^2$, with $\mathbf{r}^2$ standing for tensorial square $\mathbf{r} \otimes \mathbf{r}$ and $\mathbb{E}[\cdot]$ denoting the expectation operator. The successive states of the chain are denoted by χ_h with $h \in \mathbb{N}$ or $\mathbb{Z}$. The displacement vector after ℓ transitions, $\sum_{h=0}^{\ell-1} \mathbf{d}(\chi_h, \chi_{h+1})$, is simply written $\mathbf{r}_{0\to\ell}$ in the following. The expected square displacement divided by twice the elapsed time is written

$$\mathbb{D}_\ell[\mathbf{d}] = \frac{1}{2}\frac{\mathbb{E}[\mathbf{r}_{0\to\ell} \otimes \mathbf{r}_{0\to\ell}]}{\mathbb{E}[t_{0\to\ell}]} = \frac{1}{2}\frac{\mathbb{V}[\mathbf{r}_{0\to\ell}]}{\mathbb{E}[t_{0\to\ell}]}. \tag{1}$$

The asymptotic limit yields the diffusion matrix, i.e., $\mathbb{D}[\mathbf{d}] = \lim_{\ell\to\infty} \mathbb{D}_\ell[\mathbf{d}]$. The variance amounts to squaring here because the expected displacement $\mathbb{E}[\mathbf{r}_{0\to\ell}]$ is zero at equilibrium. The Markov chain obeys detailed balance with respect to an equilibrium stationary distribution $\rho_\chi^{\rm eq}$. Fulfillment of this strong condition entails the invariance of expectations under arbitrary translation of chain indices and under chain reversal. Expected autocorrelations are thus invariant after interchange of displacements: $\mathbb{E}[\mathbf{r}_{0\to1} \otimes \mathbf{r}_{h\to h+1}]$ is successively equal to $\mathbb{E}[\mathbf{r}_{-1-h\to-h} \otimes \mathbf{r}_{-1\to0}]$, $\mathbb{E}[\mathbf{r}_{h+1\to h} \otimes \mathbf{r}_{1\to0}]$, and eventually $\mathbb{E}[\mathbf{r}_{h\to h+1} \otimes \mathbf{r}_{0\to1}]$, displacements being antisymmetrical under chain reversal: $\mathbf{r}_{h+1\to h} = -\mathbf{r}_{h\to h+1}$, $\forall\, h$.

[1] $\mathbf{d}(\chi, \chi')$ equals $\mathbf{r}' - \mathbf{r} + \arg\min \|\mathbf{r}' - \mathbf{r} + \mathbf{m}\|$, where the components m_i of argument $\mathbf{m}$ run over the multiples of the simulation supercell periods.

Hence, $\mathbb{D}[\mathbf{d}]$ is symmetric non-negative. Translational invariance also entails that the expected elapsed time is ℓ multiplied by the mean elapsed time before the next event $\bar\tau = \mathbb{E}[t_{0\to1}]$. The autocorrelation symmetry properties enable us to split the diffusion matrix into two parts:

$$\mathbb{D}[\mathbf{d}] = \mathbb{D}_1[\mathbf{d}] + \frac{1}{\bar\tau}\sum\nolimits_{h=1}^{\infty} \mathbb{E}[\mathbf{r}_{0\to1} \otimes \mathbf{r}_{h\to h+1}]. \tag{2}$$

For uncorrelated Markov chains, the *uncorrelated* part $\mathbb{D}_1[\mathbf{d}] = \mathbb{E}[\mathbf{r}_{0\to1} \otimes \mathbf{r}_{0\to1}]/2\bar\tau$ contributes to diffusion exclusively since the *correlated* part encompassing the summation vanishes. For low-dimensional spaces, $\bar\tau$ and $\mathbb{D}_1[\mathbf{d}]$ can be readily evaluated from the knowledge of $\rho_\chi^{\rm eq}$ via conditioning on the states. Let $\mathbb{E}[f(\chi_k, \chi_{k+1})|\chi_0]$ denote the conditional expectation of function $f(\chi_k, \chi_{k+1})$ given χ_0 and integer $k \geqslant 0$. The mean first-passage time (MFPT) from χ_0 then writes $\tau_0 = \mathbb{E}[t_{0\to1}|\chi_0]$ and its mean yields $\bar\tau = \mathbb{E}[\tau_0]$. Term $\mathbb{E}[\mathbf{r}_{0\to1} \otimes \mathbf{r}_{0\to1}]$ can be similarly evaluated, yielding the uncorrelated part. Evaluating the correlated part is, however, more difficult because it requires formulating and solving a Poisson equation. For this purpose, define the mean displacement from χ_1 as

$$\mathbf{e}(\chi_1) = \mathbb{E}[\mathbf{r}_{1\to2}|\chi_1] = -\mathbb{E}[\mathbf{r}_{0\to1}|\chi_1], \tag{3}$$

and the associated relaxation vector $\boldsymbol{\epsilon}(\chi_1) = \sum_{h=1}^{+\infty} \mathbb{E}[\mathbf{e}(\chi_h)|\chi_1]$ whose knowledge will give access to the correlated part of the diffusion matrix. The relaxation vector is a particular solution of the following discrete Poisson equation:

$$\boldsymbol{\epsilon}(\chi_1) = \mathbb{E}[\boldsymbol{\epsilon}(\chi_2)|\chi_1] + \mathbf{e}(\chi_1), \tag{4}$$

where χ_1 runs over the state space. The solution $\boldsymbol{\epsilon}$ is fully determined by additionally imposing $\mathbb{E}[\boldsymbol{\epsilon}] = \mathbb{E}[\mathbf{e}] = 0$. It characterizes the expected correlations

$$\begin{aligned}\mathbb{E}[\mathbf{r}_{0\to1} \otimes \boldsymbol{\epsilon}(\chi_1)] &= \sum\nolimits_{h=1}^{\infty} \mathbb{E}[\mathbb{E}[\mathbf{r}_{0\to1} \otimes \mathbf{r}_{h\to h+1}|\chi_0, \chi_1]] \\ &= \sum\nolimits_{h=1}^{\infty} \mathbb{E}[\mathbf{r}_{0\to1} \otimes \mathbf{r}_{h\to h+1}]. \end{aligned}\tag{5}$$

Combining (2) and (5) then yields the diffusion matrix

$$\begin{aligned}\mathbb{D}[\mathbf{r}_{0\to1}] &= \mathbb{D}_1[\mathbf{r}_{0\to1}] + \frac{1}{\bar\tau}\mathbb{E}[\mathbf{r}_{0\to1} \otimes \boldsymbol{\epsilon}(\chi_1)] \\ &= \frac{1}{2\bar\tau}\mathbb{E}[[\mathbf{r}_{0\to1} + \boldsymbol{\epsilon}(\chi_1)]^2 - \boldsymbol{\epsilon}^2], \end{aligned}\tag{6}$$

where the first equality is similar to Green-Kubo formulas [27,28] and symmetry is formally recovered in the second equality. Expressions in (6) are the cornerstone of variational approaches to mass transport [27–29] and serve here the purpose of improving kMC estimations via correlation splitting and conditioning.

III. CORRELATION SPLITTING AND CONDITIONING

We proceed by first writing the LTV for displacement $\mathbf{r}_{1\to2}$ with conditioning on χ_1 and rescaling with $2\bar\tau$,

$$\mathbb{D}_1[\mathbf{r}_{1\to2}] = \mathbb{E}[\mathbb{D}_1[\mathbf{r}_{1\to2}|\chi_1]] + \mathbb{D}_1[\mathbb{E}[\mathbf{r}_{1\to2}|\chi_1]], \tag{7}$$

where $\mathbb{D}_1[\mathbf{r}_{1\to2}|\chi_1] = \mathbb{V}[\mathbf{r}_{1\to2}|\chi_1]/2\bar\tau$ and the conditional variance is $\mathbb{V}[\mathbf{r}_{1\to2}|\chi_1] = \mathbb{E}[(\mathbf{r}_{1\to2})^2|\chi_1] - \mathbf{e}(\chi_1)^2$. Further

splitting the diffusion matrix (6) is then obtained through (i) inserting the LTV (7) in (6) and conditioning the expectation of $\mathbf{r}_{0\to1}\otimes\boldsymbol{\epsilon}(\chi_1)$ on χ_1; (ii) inserting the reversibility property (3); (iii) plugging the Poisson equation (4); (iv) simplifying the plugged expectation $\mathbb{E}[\mathbb{E}[\mathbf{e}(\chi_1)\otimes\boldsymbol{\epsilon}(\chi_2)|\chi_1]]$ into $\mathbb{E}[\mathbf{e}(\chi_1)\otimes\boldsymbol{\epsilon}(\chi_2)]$ using the LTE; (v) regrouping like quantities $\mathbb{D}_1[\mathbf{e}]=\mathbb{E}[\mathbf{e}^2]/2\bar{\tau}$; (vi) identifying the diffusion matrix of the conditionally expected displacements

$$\begin{aligned}\mathbb{D}[\mathbf{e}(\chi_1)] &= \mathbb{D}_1[\mathbf{e}(\chi_1)]+\frac{1}{\bar{\tau}}\mathbb{E}[\mathbf{e}(\chi_1)\otimes\boldsymbol{\epsilon}(\chi_2)]\\ &= \frac{1}{2\bar{\tau}}\mathbb{E}[[\mathbf{e}(\chi_1)+\boldsymbol{\epsilon}(\chi_2)]^2-\boldsymbol{\epsilon}^2]\end{aligned}\tag{8}$$

by analogy to expressions of Eq. (6). Both contributions (6) and (8) are measurable by kMC simulations. The resulting splitting yields the LTD

$$\mathbb{D}[\mathbf{r}_{1\to2}]=\mathbb{E}[\mathbb{D}_1[\mathbf{r}_{1\to2}|\chi_1]]-\mathbb{D}[\mathbb{E}[\mathbf{r}_{1\to2}|\chi_1]],\tag{9}$$

in which the diffusion matrix is expressed as the difference between two symmetric non-negative contributions, the *intra*correlated and *extra*correlated diffusion matrices, respectively. Intracorrelations involve consecutive displacements exclusively since $\mathbb{E}[\mathbb{D}_1[\mathbf{r}_{1\to2}|\chi_1]]=\mathbb{D}_2[\mathbf{r}_{0\to1}]$. The remaining correlations contribute to the extracorrelated part $\mathbb{D}[\mathbf{e}(\chi_0)]=-\mathbb{E}[\mathbf{r}_{0\to1}\otimes(\mathbf{r}_{1\to2}+2\sum_{h=2}^{\infty}\mathbf{r}_{h\to h+1})]/2\bar{\tau}$. The former equality arises as the particular case $\ell=2$ of a more general relationship

$$\mathbb{D}_\ell[\mathbf{d}]=\mathbb{E}[\mathbb{D}_1[\mathbf{d}|\chi]]+\tfrac{1}{\ell}\mathbb{D}_1[\mathbb{E}[\mathbf{d}|\chi]]-\frac{\ell-1}{\ell}\mathbb{D}_{\ell-1}[\mathbb{E}[\mathbf{d}|\chi]],\tag{10}$$

derived from the reversibility property (3) and the law of total covariance [42], where $\chi\equiv\chi_1$ and $\mathbf{d}\equiv\mathbf{r}_{0\to1}$. Relationship (10) bridges between the LTV at the lower extremity and the LTD obtained for $\ell\to\infty$. The LTD entails that the diffusion matrix can be estimated from mean local quantities, by plugging the expected displacements and their conditional variances given the visited states into its extracorrelated and intracorrelated parts. Besides, the LTD and bridging law are meaningful for reversible Markov chains and for any stochastic variable that is antisymmetric under chain reversal. Laws (7) and (9) also yield a Löwner partial ordering:

$$\mathbb{D}[\mathbf{d}]\leqslant\mathbb{E}[\mathbb{D}_1[\mathbf{d}|\chi]]\leqslant\mathbb{D}_1[\mathbf{d}],$$

entailing that $\mathbb{D}[\mathbf{d}]$ is better approximated by its intracorrelated part $\mathbb{D}_2[\mathbf{d}]$ than its uncorrelated part $\mathbb{D}_1[\mathbf{d}]$. Further increasing ℓ provides a decaying sequence $(\mathbb{D}_\ell[\mathbf{d}])_{\ell\geqslant1}$ of upper-bound approximates of $\mathbb{D}[\mathbf{d}]$ [29]. We then estimate $\mathbb{D}[\mathbf{d}]$ via $\mathbb{D}_\ell[\mathbf{d}]$ in (10) over a sample of l trajectories of $L=\ell_{\max}$ steps each. For statistical errors to be small, l must be large enough, standard deviations decaying as $1/\sqrt{l}$ [43]. Letting $\chi_{i,h}$ denote state h of trajectory i and $\mathbf{V}(\chi_{i,h})$ stand for $\mathbb{V}[\mathbf{r}_{i,h\to h+1}|\chi_{i,h}]$, the LTD-based conditioned estimator of $\mathbb{D}_\ell[\mathbf{d}]$ writes

$$\begin{aligned}\mathbf{D}^{\mathrm{cnd}}_{l,\ell}=&\frac{1}{2\widehat{\tau}}\frac{1}{lL}\sum_{i=1}^{l}\sum_{h=0}^{L-1}\left[\mathbf{V}(\chi_{i,h})+\frac{1}{\ell}\mathbf{e}(\chi_{i,h})^2\right]\\&-\frac{1}{2\widehat{\tau}}\frac{1}{l\ell}\sum_{i=1}^{l}\left[\sum_{h=1}^{\ell-1}\mathbf{e}(\chi_{i,h})\right]^2,\end{aligned}\tag{11}$$

where $\widehat{\tau}$ is an estimate of $\bar{\tau}$ obtained via LTE-based conditioning, i.e., by averaging the MFPTs [44,45]:

$$\widehat{\tau}=\frac{1}{lL}\sum_{i=1}^{l}\sum_{h=0}^{L-1}\mathbb{E}[t_{i,h\to h+1}|\chi_{i,h}].\tag{12}$$

Note that information about the lL gathered states is included in the estimation of static expectations in (11) and (12). Conditioned estimator in (12) has a statistical variance that is lower than that of the plain estimator $\sum_{i=1}^{l}t_{i,0\to\ell}$, a property guaranteed by the LTV [33,35,40]. The conditioning over time is traditionally done in the standard estimator of $\mathbb{D}_\ell[\mathbf{d}]$:

$$\mathbf{D}^{\mathrm{std}}_{l,\ell}=\frac{1}{2\widehat{\tau}}\frac{1}{l\ell}\sum_{i=1}^{l}\mathbf{r}_{i,0\to\ell}\otimes\mathbf{r}_{i,0\to\ell}.\tag{13}$$

While estimators (11) and (13) are both valid, their statistical variances usually differ. Hereafter, the optimal linear combination of the standard and conditioned estimators will be employed as a third estimator, as in waste-recycling Monte Carlo [32,38], because it provides maximum reduction of the statistical variance via a control variate [43].

Consider a mobile defect evolving randomly on a flat potential energy surface. Its conditional mean displacements $\mathbf{e}(\chi)$ are all zero and its conditional variances $\mathbf{V}(\chi)$ all equal a same constant matrix $\tilde{\mathbf{V}}$. For all generated trajectories, the conditioned estimator yields $\tilde{\mathbf{V}}/2\bar{\tau}$, the exact diffusion matrix of the defect. In this trivial situation, the conditioned estimator is the perfect zero-variance estimator whereas the standard estimator has nonzero statistical variance. Statistical errors of the conditioned estimator occur when the transition rates of mobile defects differ and their atomic environment also evolves. Thus, the interesting question to address is how the three estimators behave when the spectrum of the hopping rates is extremely broad, that is, when severe kinetic trapping of the mobile defect is observed in the Monte Carlo simulations.

IV. AUXILIARY ABSORBING MARKOV CHAINS

Correlation splitting and conditioning can be employed in conventional or advanced kMC simulations. Here, we present simulations of severe kinetic trapping using the kinetic path sampling (kPS) algorithm [46–48]. kPS is an accelerated kMC algorithm developed upon theories of absorbing Markov chains (AMC) and graph transformation [49]. It performs nonlocal displacements avoiding the most trapping states. Those are formally pooled together into a prespecified set, called *transient set* using AMC terminology and denoted by $\mathtt{T}$. Moreover, kPS algorithm is able to generate first-passage paths and times efficiently based on matrix factorizations or inversions. Other AMC-kMC algorithms rely either on matrix diagonalizations [50–55], a mean rate ersatz [44,45] based on Eq. (12), or an on-the-fly modification of the hopping rates [56]. The kMC and kPS stochastic matrices, respectively denoted by P^{o} and P, satisfy the conditions $P^{\mathrm{o}}_{\chi\chi}=0$ and $P_{\chi\zeta}=0,\forall\,\chi,\forall\,\zeta\in\mathtt{T}\cup\{\chi\}$. The probabilities of not transitioning are always zero from any state and the respective MFPTs, denoted by τ^{o}_χ and τ_χ, are state dependent. Matrix P is constructed from P^{o} and an absorbing stochastic matrix, P^{a} coinciding with P^{o} over $\mathtt{T}$ and with identity matrix I over $\bar{\mathtt{T}}$, the complement of $\mathtt{T}$. This entails that transitions from $\bar{\mathtt{T}}$ are canceled, making $\mathtt{T}$ states

transient and $\bar{\mathtt{T}}$ states absorbing:

$$P^{\mathrm{a}}_{\chi\chi'} = \mathbf{1}_{\mathtt{T}}(\chi)P^{\mathrm{o}}_{\chi\chi'} + \mathbf{1}_{\bar{\mathtt{T}}}(\chi)I_{\chi\chi'}, \tag{14}$$

where indicator function $\mathbf{1}_{\mathtt{S}}$ is 1 if $\chi \in \mathtt{S}$ and 0 otherwise. Resorting to AMC theory [44–53], the mean number of visits of transient state ζ' is defined as the conditional expectation of the indicator function $\mathbf{1}_{\{\zeta'\}}$ given initial state $\chi_1 \in \mathtt{T}$. It corresponds to the Green function $\chi_1 \mapsto G^{\mathrm{a}}_{\chi_1\zeta'} = \sum_{k=0}^{\infty} \mathbb{E}^{\mathrm{a}}[\mathbf{1}_{\{\zeta'\}}(\chi_{k+1})|\chi_1]$ solution of the Poisson equation over $\mathtt{T}$:

$$G^{\mathrm{a}}_{\chi_1\zeta'} = \mathbb{E}^{\mathrm{a}}\big[G^{\mathrm{a}}_{\chi_2\zeta'}|\chi_1\big] + \mathbf{1}_{\{\zeta'\}}(\chi_1), \tag{15}$$

entailing $G^{\mathrm{a}}_{\zeta\zeta'} = \sum_{\xi\in\mathtt{T}} P^{\mathrm{o}}_{\zeta\xi}G^{\mathrm{a}}_{\xi\zeta'} + I_{\zeta\zeta'}$, while $G^{\mathrm{a}}_{\chi\chi'}$ is set to zero whenever χ or χ' lies outside $\mathtt{T}$. Thus, G^{a} and $I - P^{\mathrm{a}}$ are two singular matrices, pseudoinverse of each other, whereas $G^{\mathrm{a}}_{\zeta\zeta'}$ is the regular inverse of $I_{\zeta\zeta'} - P^{\mathrm{a}}_{\zeta\zeta'}$ for $\zeta, \zeta' \in \mathtt{T}$. For an absorbing Markov chain starting from ζ, the knowledge of the number of visits of state ζ' enables one to deduce the probability of being absorbed at $\chi' \in \bar{\mathtt{T}}$ and the mean time for being absorbed in $\bar{\mathtt{T}}$:

$$\begin{aligned} \Pi^{\mathrm{a}}_{\zeta\chi'} &= \sum\nolimits_{\zeta'} G^{\mathrm{a}}_{\zeta\zeta'}P^{\mathrm{a}}_{\zeta'\chi'} + I_{\zeta\chi'}, \\ \tau^{\mathrm{a}}_{\zeta} &= \sum\nolimits_{\zeta'} G^{\mathrm{a}}_{\zeta\zeta'}\tau^{\mathrm{o}}_{\zeta'}. \end{aligned} \tag{16}$$

The overlying transition probability from χ to $\chi' \neq \chi$ and the MFPT from χ eventually write

$$\begin{aligned} P_{\chi\chi'} &= \sum\nolimits_{\zeta} P^{\mathrm{o}}_{\chi\zeta}\Pi^{\mathrm{a}}_{\zeta\chi'}/\pi_{\chi}, \\ \tau_{\chi} &= \sum\nolimits_{\zeta} P^{\mathrm{o}}_{\chi\zeta}\big(\tau^{\mathrm{o}}_{\chi} + \tau^{\mathrm{a}}_{\zeta}\big)/\pi_{\chi}, \end{aligned} \tag{17}$$

where rescaling of both transition probabilities and elapsed times by probability $\pi_{\chi} = 1 - \sum_{\zeta} P^{\mathrm{o}}_{\chi\zeta}\Pi^{\mathrm{a}}_{\zeta\chi}$ serves to cancel the flicker probability, thus, $P_{\chi\chi} = 0$. Besides, if $P^{\mathrm{o}}_{\chi\chi'}$ obeys detailed balance with respect to its stationary probability distribution ρ^{o}_{χ} over $\bar{\mathtt{T}} \cup \mathtt{T}$, then so does $P_{\chi\chi'}$ with respect to $\rho_{\chi} \propto \rho^{\mathrm{o}}_{\chi}\pi_{\chi}$ over $\bar{\mathtt{T}}$. The scaled probability distribution $\rho^{\mathrm{eq}}_{\chi} \propto \rho^{\mathrm{o}}_{\chi}\tau^{\mathrm{o}}_{\chi} \propto \rho_{\chi}\tau^{\mathrm{o}}_{\chi}/\pi_{\chi}$ then corresponds to the thermodynamic equilibrium. Fulfilment of the reversibility property allows conditioning to be performed. The conditioned estimator (11) can thus be used. Note that the kPS algorithm reverts to the conventional kMC algorithm when none of the states are made transient.

V. RANDOM ALLOY MODEL

We illustrate the approach by computing the mass transport coefficients in a random binary alloy on a square lattice with periodic conditions. Diffusion is mediated by a single vacancy V exchanging with A or B nearest-neighbor atoms [3,29,57]. As aforementioned, transition rates are usually computed in the framework of transition state theory [7]. They have the classical form $\nu_X = \nu^{\star}\exp[-E_X/(k_BT)]$ where $E_X > 0$ is the energy barrier that neighboring atom X jumping into the vacancy must cross and $\nu^{\star}$ is the attempt frequency for both species. Here, transition rates are environment independent and only depend on the type of the jumping atom. Consequently, all states are equiprobable, and the system energy has same constant value for all stable states. No thermodynamic transition occurs in the random solid solution [3]. In particular, the site percolation threshold is independent of the jumping frequencies ν_A and ν_B. Despite its simplicity, the random alloy model is a nontrivial system and is thus customarily used to study trapping and percolation [29,57]. Assuming $E_A > E_B > 0$, the frequency ratio ν_B/ν_A increases with decreasing the temperature. Hence, low temperatures result in dynamical trapping. Here, the jump rate of B atoms, ν_B, will be much higher than the one of A atoms, ν_A. For the sake of simplicity, we adopt ν_A units by setting this value to 1 in the following. To perform kPS simulations, the transient graph is to be crafted as the union of many disconnected subgraphs, so that relatively small blocks of $I - P^{\mathrm{a}}$ need being numerically manipulated on the fly (for computing Π^{a} and τ^{a}). We illustrate the construction of the simulated networks on a square lattice in Fig. 1. Trapping is suppressed by making transient all the states where the vacancy is located next to a B atom. The difficulty is that vacancy-solute cluster shapes are connected to each other [see Fig. 1(a)], rendering the size of the local transient block so huge that its enumeration is numerically impracticable except for small and isolated B clusters. The problem is mitigated by first augmenting the transition network through the insertion of saddle states along AV exchanges to divide the trapping network into many disconnected subgraphs [see Fig. 1(b)]. Transition probabilities from any added saddle state to its two adjacent stable states both equal half. Besides, doubling the transition rates from a stable state to its adjacent saddle states and nullifying the residence times τ^{o} at the added saddles compensates the effect of the occasional flickers between stable and saddle states. Finally, stable states are all turned transient, as diagramed in Fig. 1(c). That is, set $\mathtt{T}$ is the space of stable states and the simulated network $\bar{\mathtt{T}}$ exclusively consists of the inserted saddle states. The augmentation or reduction of the network leaves the distributions of the sequences of simulated events and times unaffected.

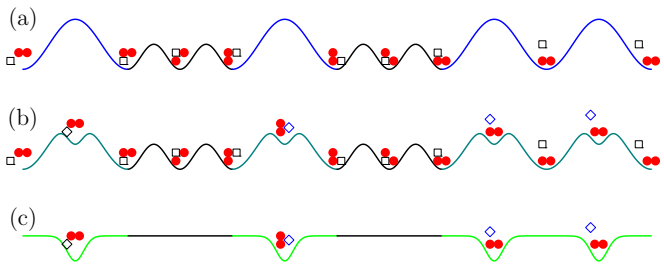


FIG. 1. Transformation of transition networks: (a) physical network wherein blue and black barriers map out exchanges of a vacancy (empty squares) with bulk A atoms (not displayed) or solute B atoms (red disks); (b) augmented network after inserting saddle states along vacancy-A exchanges (empty diamonds represent vacancies at saddle positions); (c) reduced network after eliminating stable states

Computing the conditional cumulants given the sampled states in estimator (11) is strenuous when a solute cluster, i.e., a subgraph of the transient network, percolates through the periodically replicated supercell, as illustrated in Fig. 2. Cumulants $\mathbf{e}(\chi_0)$ and $\mathbf{V}(\chi_0)$ must account for all the

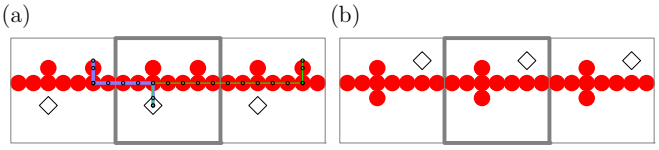


FIG. 2. A supercell (in bold) is periodically replicated horizontally. The blue and green paths represent two distinct sequences of atomic displacements through the percolating solute cluster (the transient subgraph) between the same starting state in (a) and ending state in (b).

displacements $\mathbf{r}_{0\to1}$ possibly sampled by kPS algorithm. The sampled displacements starting in χ_0 and ending in $\chi_1 \in \bar{\mathtt{T}}$ are all congruent to $\mathbf{d}(\chi_0, \chi_1)$ modulo the cell periods along the percolating directions [see Fig. 2(a)], and many among them may differ from $\mathbf{d}(\chi_0, \chi_1)$. This consequent sampling burden is avoided by analytically integrating the underlying conditional expected displacements $\mathbf{e}^{\mathrm{a}}(\chi_h) \triangleq \mathbb{E}^{\mathrm{a}}[\mathbf{r}^{\mathrm{u}}_{h\to h+1}|\chi_h]$, in a similar way to [15,47]. Letting $\mathbb{E}^{\mathrm{o}}[\cdot]$ denote expectation with respect to P^{o}, both cumulants of overlying displacement $\mathbf{r}_{0\to1}$ are determined by the underlying sequences $\mathbf{r}^{\mathrm{u}}_{0\to1} + \mathbf{r}^{\mathrm{u}}_{1\to\infty} \equiv \mathbf{r}_{0\to1}$ associated with the successive states of the AMC, $\{\chi^{\mathrm{u}}_h\}_{h\geqslant1}$, and where $\chi^{\mathrm{u}}_0 = \chi_0$ and $\chi^{\mathrm{u}}_\infty = \chi_1$.

Conditioning after the P^{o} transition within decomposition (17) yields

$$\mathbf{e}(\chi_0) = \mathbb{E}^{\mathrm{o}}\big[\mathbf{r}^{\mathrm{u}}_{0\to1} + \mathbb{E}^{\mathrm{a}}\big[\mathbf{r}^{\mathrm{u}}_{1\to\infty}|\chi_1\big]\big|\chi_0\big]/\pi_{\chi_0}, \tag{18a}$$

$$\mathbf{V}(\chi_0) = \mathbb{E}^{\mathrm{o}}\big[\big[\mathbf{r}^{\mathrm{u}}_{0\to1} + \mathbb{E}^{\mathrm{a}}\big[\mathbf{r}^{\mathrm{u}}_{1\to\infty}|\chi_1\big] - \mathbf{e}(\chi_0)\big]^2\big|\chi_0\big]/\pi_{\chi_0}. \tag{18b}$$

The mean displacement $\mathbb{E}^{\mathrm{a}}[\mathbf{e}^{\mathrm{a}}]$ being null, the relaxation vector $\boldsymbol{\epsilon}^{\mathrm{a}}(\chi_1) \triangleq \mathbb{E}^{\mathrm{a}}[\mathbf{r}_{1\to\infty}|\chi_1] = \sum_{h=1}^{+\infty}\mathbb{E}^{\mathrm{a}}[\mathbf{e}^{\mathrm{a}}(\chi_h)|\chi_1]$, is null outside $\mathtt{T}$ and satisfies a Poisson equation inside $\mathtt{T}$:

$$\boldsymbol{\epsilon}^{\mathrm{a}}(\chi_1) = \mathbb{E}^{\mathrm{a}}[\boldsymbol{\epsilon}^{\mathrm{a}}(\chi_2)|\chi_1] + \mathbf{e}^{\mathrm{a}}(\chi_1). \tag{19}$$

The solution is unique, and reads as $\boldsymbol{\epsilon}^{\mathrm{a}}(\zeta) = \sum_{\zeta'} G^{\mathrm{a}}_{\zeta\zeta'}\mathbf{e}^{\mathrm{a}}(\zeta')$ for $\zeta \in \mathtt{T}$ and cancels outside $\mathtt{T}$. It serves to evaluate the two conditional cumulants (18) for estimator (11). We resort to their respective LTE and LTV expressions with conditioning over the underlying absorbing chain initiated from $\zeta \equiv \chi_1$ to obtain a numerically tractable expression

$$\mathbf{e}(\chi) = \sum\nolimits_{\zeta}[\mathbf{d}(\chi,\zeta) + \boldsymbol{\epsilon}^{\mathrm{a}}(\zeta)]P^{\mathrm{o}}_{\chi\zeta}/\pi_\chi, \tag{20a}$$

$$\mathbf{V}(\chi) = \sum\nolimits_{\zeta}\big\{\mathbf{V}^{\mathrm{a}}(\zeta) + [\mathbf{d}(\chi,\zeta) + \boldsymbol{\epsilon}^{\mathrm{a}}(\zeta) - \mathbf{e}(\chi)]^2\big\}P^{\mathrm{o}}_{\chi\zeta}/\pi_\chi, \tag{20b}$$

where $\chi \equiv \chi_0$ in (18). The variance of the absorbing chain conditioned on $\zeta \equiv \chi_1$ is also computed using the Green function and relaxation vectors, resorting to relation (22) below:

$$\begin{aligned}\mathbf{V}^{\mathrm{a}}(\chi_1) &= \mathbb{E}^{\mathrm{a}}\Big[\Big(\sum\nolimits_{h=1}^{\infty}\mathbf{r}^{\mathrm{u}}_{h\to h+1}\Big)^2\Big|\chi_1\Big] - \boldsymbol{\epsilon}^{\mathrm{a}}(\chi_1)^2 \qquad (21)\\ &= \sum\nolimits_{h=1}^{\infty}\mathbb{E}^{\mathrm{a}}\big[(\mathbf{r}^{\mathrm{u}}_{h\to h+1} + \boldsymbol{\epsilon}^{\mathrm{a}}(\chi_{h+1}))^2 - \boldsymbol{\epsilon}^{\mathrm{a}}(\chi_h)^2\big|\chi_1\big]\\ &= \sum\nolimits_{\chi\zeta} G^{\mathrm{a}}_{\chi_1\chi}\big\{P^{\mathrm{a}}_{\chi\zeta}[\mathbf{d}(\chi,\zeta) + \boldsymbol{\epsilon}^{\mathrm{a}}(\zeta)]^2 - \boldsymbol{\epsilon}^{\mathrm{a}}(\chi)^2\big\}. \qquad (22)\end{aligned}$$

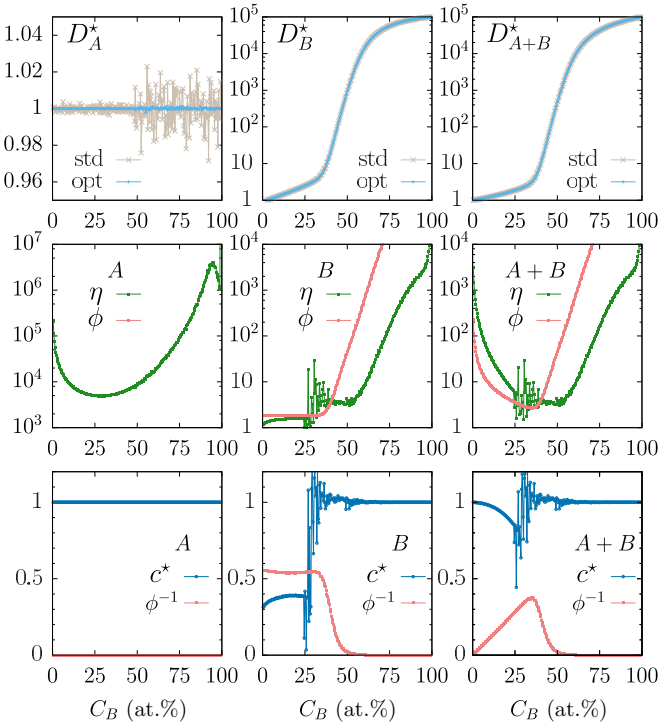


FIG. 3. Atomic diffusivities $D^\star_X$ ($X = A$, B, and $A + B$) for extreme dynamical trapping ($\nu_A = 1$ and $\nu_B = 10^5$), as a function of C_B, with corresponding variance reduction factor η, intracorrelation-to-extracorrelation ratio ϕ, and optimal variate $c^\star$. The supercell size is 16×16.

Note that quantities $\boldsymbol{\epsilon}^{\mathrm{a}}$ and $\mathbf{V}^{\mathrm{a}}$ are first and second derivatives of a displacement cumulant generating function at its origin, respectively [15].

VI. ESTIMATION OF THE DIFFUSION COEFFICIENTS

We perform a series of kPS simulations of extreme dynamical trapping by setting $\nu_B = 10^5$ and $\nu_A = 1$ in a periodically replicated square lattice of size 16×16. Compositions are gradually increased from 1 to 254 B atoms. The atomic concentration of X is denoted by C_X, entailing that $C_{A+B} = C_A + C_B$ is one. The diffusion matrix $\mathbb{D}[\mathbf{d}]$ is estimated using $\mathbf{D}^{\mathrm{std}}_{l,L}$ and $\mathbf{D}^{\mathrm{cnd}}_{l,L}$ estimators with $L = \ell_{\max} = 200$, $l = 5 \times 10^5$ for $C_B < 0.5$, and $l = 10^4$ for $C_B \geqslant 0.5$. Estimates D^{std}_X and D^{cnd}_X of the diffusion coefficients D_X for both species and the vacancy ($X = A$, B, and $A + B$) are then obtained via $\mathbf{D}^{\mathrm{std}}_{l,L}$ and $\mathbf{D}^{\mathrm{cnd}}_{l,L}$ by averaging the corresponding elements over the two space directions. The optimal estimate is then obtained as $D^{\mathrm{opt}}_X = (1 - c^\star)D^{\mathrm{std}}_X + c^\star D^{\mathrm{cnd}}_X$ where the optimal control variate is $c^\star = -\mathrm{cov}(D^{\mathrm{std}}_X, D^{\mathrm{cnd}}_X - D^{\mathrm{std}}_X)/\mathrm{var}(D^{\mathrm{cnd}}_X - D^{\mathrm{std}}_X)$. We furthermore record the transient regimes $D^{\mathrm{cnd}}_X(\ell) = \Sigma_\ell + \frac{1}{\ell}\Gamma_1 + \frac{1-\ell}{\ell}\Gamma_{\ell-1}$ from (10) where Σ_ℓ and $\Gamma_{\ell-1}$ are estimates of the corresponding intracorrelated and extracorrelated parts. Last, we define and evaluate the intracorrelation-to-extracorrelation ratio $\phi = \Sigma_L/\Gamma_L$ and the reduction factor of the statistical variance $\eta = \mathrm{var}(D^{\mathrm{std}}_X)/\mathrm{var}(D^{\mathrm{opt}}_X)$.

The atomic diffusivities $D^\star_X = D_X/C_X$ evaluated using the standard and optimal estimators for the entire composition range are displayed in Fig. 3, together with η, ϕ, and $c^\star$. We

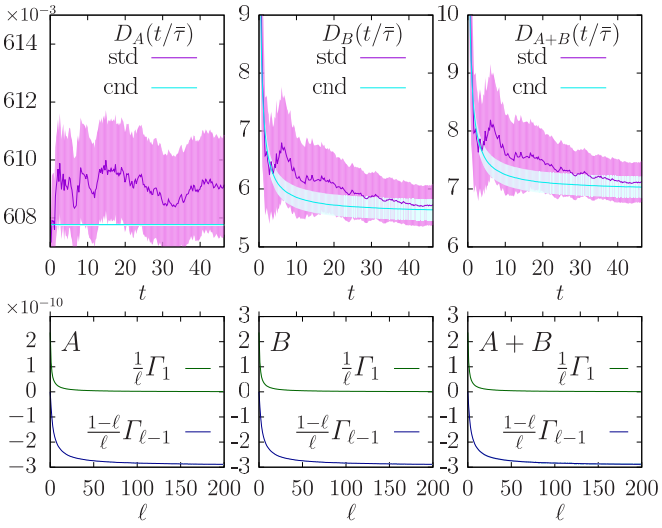


FIG. 4. Time dependence of the estimated $D_X(\ell)$ with $\ell = t/\bar{\tau}$, using standard (13) and conditioned (11) estimators, for $X = A$, B, and $A + B$. Filled areas around the curves represent 95% confidence intervals (CI). CIs around $\frac{1}{\ell}\Gamma_1$ and $\frac{1-\ell}{\ell}\Gamma_\ell$ curves are too small to be visible.

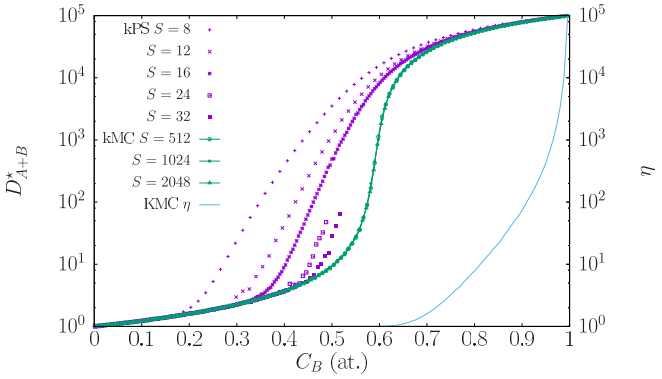


FIG. 5. Diffusion coefficient D_{A+B} as a function of composition for various lattice sizes S using the kPS and kMC algorithms. The optimized estimator is used in all calculations. The kPS simulations are performed with same setup as in Fig. 3, but four additional supercell sizes, $S = 8$, 12, 24, and 32. The conventional kMC simulations employ 10^4 trajectories of 10^6 steps. Their CPU costs are almost independent of the system sizes. Note that the speedups η obtained through conditioning are considerable in conventional kMC simulations of dilute A_xB_{1-x} systems with $x < 0.1$.

observe that the speedup measured in terms of η is considerable whenever the intracorrelated contribution to diffusivity dominates ($\phi \gg 1$). In this situation, the optimal estimator perfectly matches the conditioned estimator ($c^\star = 1$). The optimal estimator is relatively less efficient for the fast-diffusing B atoms when the extracorrelated contribution to B diffusivity is significant, at B concentration lower than 40%. The lowest reductions of variance are about a factor of 2. To investigate the origin of the relatively lower performance of the conditioned estimator, we display in Fig. 4 the transient regime estimated from $D_X^{\rm std}(\ell)$, $D_X^{\rm cnd}(\ell)$, and $\Gamma_{\ell-1}$ with estimates of their standard errors for $0 \leqslant \ell \leqslant \ell_{\rm max}$. The errors associated with $\Gamma_{\ell-1}$ terms are negligible compared to those with Σ_ℓ terms and are attributed to the intermittent binding of the vacancy to the B clusters. Removing this intermittency in the kPS algorithm would require making additional states transient and handling A-connected subgraphs similarly to B clusters.

Interestingly, the negative contributions $\frac{1-\ell}{\ell}\Gamma_\ell$ in Fig. 4 undergo fast algebraic decays towards their plateau values δ. The three curves are very well fitted by a law of the form $g(\ell + \ell_0)^\alpha + \delta$. Implementing the nonlinear least-squares Marquardt-Levenberg algorithm with the four fitting parameters g, ℓ_0, α, and δ yields the power-law exponents α associated with A, B, and $A + B$ diffusivities. The obtained α values lie in the following 68%-confidence intervals: -1.302 ± 0.091, -1.015 ± 0.008, and -1.015 ± 0.008, respectively. The convergence features of the mean-squared mean displacements entail that a standard diffusive regime exhibiting short-range dependence is quickly reached as ℓ increases [58]. This property is related to the fast algebraic decay of the autocorrelation function, as detailed in [42]. Note that the larger exponent associated with A diffusivity decreases as the frequency ratio is decreased [42]. This physical trend results from a nontrivial interplay between composition, transition rates, site interactions, and geometry. We refer to the recent work of Settino *et al.* [59] who studied anomalous diffusion in the Aubry-André model via the autocorrelation functions and investigated the dependence of their power-law decay on the model physical parameters.

Here, the extremely severe dynamical trapping of the vacancy with B atoms strongly impacts the monotonous increase of B diffusivity with C_B. The sudden sharp increase of $D_B^\star$ observed at $C_B \approx 0.35$ occurs at a concentration much lower than $p_s = 0.592\,745$, the site percolation threshold [60]. This dynamical transition is due to the cooperative motion of small B clusters whose effectiveness increases considerably with C_B in small supercells. With increasing supercell sizes, the transition further sharpens and occurs closer to the percolation threshold, as shown in Fig. 5.

The kPS simulations for the two largest supercell sizes in Fig. 5 became inefficient and were stopped before terminating. The inefficiency results from the larger sizes of the percolating solute clusters and to the cost of computing the Green functions for the associated transient subgraphs, a task involving matrix inversion or factorization. Here, a direct nonoptimized dense solver was used whose complexity scales cubically with the sizes of the transient subgraphs. As a result, the approach starts consuming CPU time enormously when supercell sizes and B concentrations are too large. Nevertheless, dynamical trapping disappearing beyond the percolation threshold, conventional kMC simulations can be used instead. One then obtains reliable estimates of the diffusion coefficients at much larger system sizes, as shown in Fig. 5. The variance reduction factor η allowed by the optimal estimator in kMC simulations increases from 1 below the percolation threshold to 10^5 in pure B. For concentrated alloy system $A_{0.1}B_{0.9}$, the factor of variance reduction η is 10^2, yielding an appreciable speedup. However, the conditioned estimator underperforms the standard one at the low-B concentrations, when trapping becomes important in conventional

kMC simulations. Results obtained using the conventional kMC algorithm in systems exhibiting moderate dynamical trapping are also reported in [42], where it is shown that significant variance reductions via conditioning are systematically observed. The conventional kMC algorithm outperforms kPS algorithm with excessively large transient subgraphs because the trapping strength measured in number of steps the vacancy remains attached to a solute cluster scales linearly with the cluster size, while the factorization cost scales cubically here. A smaller prefactor for the factorization costs makes kPS advantageous for transient subgraphs smaller than a certain threshold value. Hence, there are two complementary ways to improve kPS simulations: (i) avoid turning a large vacancy-solute cluster into a transient subgraph when its size is above the threshold, (ii) resort to a sparse linear solver to reduce the factorization and inversion costs. The latter costs grow quadratically with the subgraph sizes for the direct multifrontal linear solver used in Ref. [47].

Nonetheless, an interesting trend emerges from the results of the kPS simulations with severe trapping. We indeed observe that the extracorrelation-to-intracorrelation ratio ϕ^{-1} vanishes for all diffusion measurements reported in Fig. 3 when the solute concentrations are larger than the dynamical percolation threshold values. This property means that the correlations of the underlying process are well captured by the auxiliary absorbing Markov chains. It entails that the extracorrelated part of the diffusion matrix is negligible and justifies the use of the kinetic cluster expansion (KineCluE) method [24] to solve this particularly difficult diffusion problem. This method neglects the extracorrelated part and similarly resorts to auxiliary absorbing Markov chains, but these ones are constructed from a subgraph expansion. To adapt the KineCluE method to concentrated alloys, the absorbing Markov chains should be solved for a sample of alloy configurations generated at thermodynamic equilibrium. Whenever the extracorrelated part containing the cluster correlations is negligible, the transport coefficients may be correctly estimated from their intracorrelated contributions exclusively.

Concerning the transport properties of the slowly migrating solvent species, we observe that A diffusivity is almost not impacted by dynamical trapping and remains constant. Reproducing a sluggish diffusion behavior where A diffusivity exhibits a minimum at intermediate compositions, as observed experimentally in several concentrated solid solution alloys [44] and highly debated in the literature on high-entropy alloys [61–66], will necessitate to parametrize the exchange rates ν_A and ν_B, for instance, by accounting for the binding energies and entropies between alloying elements and vacancies [14,18,19,67]. This would affect short-range ordering or clustering, introduce a dependency of vacancy concentration on alloy composition, and impact atomic diffusion.

VII. CONCLUSION

Splitting the diffusion matrix into its intracorrelated and extracorrelated parts and conditioning the correlations enables one to formulate a law of total diffusion. A conditioned estimator then allows measuring atomic diffusivities with considerably improved accuracy in absence of dynamical trapping. The use of an optimized control variate guarantees systematic variance reductions compared with standard computations performed with conventional or advanced kinetic Monte Carlo methods. Conditioning is particularly useful when the latter methods employ auxiliary absorbing Markov chains able to suppress trapping at the underlying scale, like kinetic path sampling, as it leverages the Green functions that are computed to generate the escaping first-passage paths. However, the cost of computing these Green functions must remain reasonable so that kinetic path sampling simulations always outperforms conventional kinetic Monte Carlo simulations. If this condition is not met, it is preferable to limit the sizes of the transient subgraphs or to revert to conventional kMC simulations. The conditioning approach is in principle amenable to the numerous kMC simulations dealing with realistic potential energy surface accounting for lattice distortions [19] or describing amorphous structures [68]. In these simulations, the computation of the transition rates is often so costly that the number of simulated events is quite limited. The variance reduction technique proposed here will certainly be useful in this particular context. As the conditioning approach represents a small overhead, it can be readily applied to estimate transport properties of any particles migrating through thermally activated events in crystalline or noncrystalline solids. Its range of applicability encompasses surface and bulk diffusion in presence of extended defects [47,69–71] like cavities, clusters, dislocations, or grain boundaries, within complex alloys or any material compounds.

ACKNOWLEDGMENTS

Stimulating discussions with V. Bulatov, B. Jourdain, M. Nastar, K. Mallick, and D. Trinkle are gratefully acknowledged.

[1] D. Chandler, *Introduction to Modern Statistical Mechanics* (Oxford University Press, Oxford, 1987).

[2] D. J. Evans and G. P. Morriss, *Statistical Mechanics of Nonequilibrium Liquids* (ANU Press, Canberra, 2007).

[3] A. R. Allnatt and A. B. Lidiard, *Atomic Transport in Solids* (Cambridge University Press, Cambridge, 1993).

[4] H. Mehrer, *Diffusion Mechanisms* (Springer, Berlin, 2007), pp. 95–104.

[5] S. Zhao, Y. Osetsky, and Y. Zhang, Preferential diffusion in concentrated solid solution alloys: NiFe, NiCo and NiCoCr, Acta Mater. **128**, 391 (2017).

[6] Y. Osetsky, A. V. Barashev, L. K. Béland, Z. Yao, K. Ferasat, and Y. Zhang, Tunable chemical complexity to control atomic diffusion in alloys, npj Comput. Mater. **6**, 38 (2020).

[7] P. Hänggi, P. Talkner, and M. Borkovec, Reaction-rate theory: Fifty years after Kramers, Rev. Mod. Phys. **62**, 251 (1990).

[8] P. Terrier, M.-C. Marinica, and M. Athènes, Using bayes formula to estimate rates of rare events in transition path sampling simulations, J. Chem. Phys. **143**, 134121 (2015).

[9] K. Arakawa, M.-C. Marinica, S. Fitzgerald, L. Proville, D. Nguyen-Manh, S. L. Dudarev, P.-W. Ma, T. D. Swinburne,

A. M. Goryaeva, T. Yamada *et al.*, Quantum de-trapping and transport of heavy defects in tungsten, Nat. Mater. **19**, 508 (2020).

[10] A. Agarwal, N. W. Hengartner, S. Gnanakaran, and A. F. Voter, Computing long time scale biomolecular dynamics using quasi-stationary distribution kinetic Monte Carlo (qsd-kmc), J. Chem. Phys. **151**, 074109 (2019).

[11] Y. Osetsky, D. Bacon, A. Serra, B. Singh, and S. Golubov, Stability and mobility of defect clusters and dislocation loops in metals, J. Nucl. Mater. **276**, 65 (2000).

[12] D. A. Terentyev, L. Malerba, and M. Hou, Dimensionality of interstitial cluster motion in bcc-fe, Phys. Rev. B **75**, 104108 (2007).

[13] C. Le Bris, T. Lelièvre, M. Luskin, and D. Perez, A mathematical formalization of the parallel replica dynamics, Monte Carlo Methods Appl. **18**, 119 (2012).

[14] T. D. Swinburne and D. Perez, Self-optimized construction of transition rate matrices from accelerated atomistic simulations with bayesian uncertainty quantification, Phys. Rev. Materials **2**, 053802 (2018).

[15] T. D. Swinburne and D. Perez, Automated calculation and convergence of defect transport tensors, npj Comput. Mater. **6**, 190 (2020).

[16] J.-M. Lanore, Simulation de l'évolution des défauts dans un réseau par la méthode de Monte-Carlo, Radiat. Eff. **22**, 153 (1974).

[17] A. Bortz, M. Kalos, and J. Lebowitz, A new algorithm for monte carlo simulation of ising spin systems, J. Comput. Phys. **17**, 10 (1975).

[18] M. Trochet, A. Sauvé-Lacoursière, and N. Mousseau, Algorithmic developments of the kinetic activation-relaxation technique: Accessing long-time kinetics of larger and more complex systems, J. Chem. Phys. **147**, 152712 (2017).

[19] M. Trochet, N. Mousseau, L. K. Béland, and G. Henkelman, *Off-Lattice Kinetic Monte Carlo Methods* (Springer, Cham, 2019), pp. 1–29.

[20] M. Koiwa and S. Ishioka, Integral methods in the calculation of correlation factors for impurity diffusion, Philos. Mag. A **47**, 927 (1983).

[21] M. Nastar, Atomic diffusion theory challenging the Cahn-Hilliard method, Phys. Rev. B **90**, 144101 (2014).

[22] J.-L. Bocquet, Correlation factor for diffusion in cubic crystals with solute-vacancy interactions of arbitrary range, Philos. Mag. **94**, 3603 (2014).

[23] V. G. Vaks, K. Y. Khromov, I. R. Pankratov, and V. V. Popov, Statistical theory of diffusion in concentrated bcc and fcc alloys and concentration dependencies of diffusion coefficients in bcc alloys FeCu, FeMn, FeNi, and FeCr, J. Exp. Theor. Phys. **123**, 59 (2016).

[24] T. Schuler, L. Messina, and M. Nastar, Kineclue: A kinetic cluster expansion code to compute transport coefficients beyond the dilute limit, Comput. Mater. Sci. **172**, 109191 (2020).

[25] D. R. Trinkle, Automatic numerical evaluation of vacancy-mediated transport for arbitrary crystals: Onsager coefficients in the dilute limit using a Green function approach, Philos. Mag. **97**, 2514 (2017).

[26] R. Agarwal and D. R. Trinkle, Exact Model of Vacancy-Mediated Solute Transport in Magnesium, Phys. Rev. Lett. **118**, 105901 (2017).

[27] C. Arita, P. L. Krapivsky, and K. Mallick, Variational calculation of transport coefficients in diffusive lattice gases, Phys. Rev. E **95**, 032121 (2017).

[28] C. Arita, P. L. Krapivsky, and K. Mallick, Bulk diffusion in a kinetically constrained lattice gas, J. Phys. A: Math. Theor. **51**, 125002 (2018).

[29] D. R. Trinkle, Variational Principle for Mass Transport, Phys. Rev. Lett. **121**, 235901 (2018).

[30] M. Duflo, *Random Iterative Models* of Applications of Mathematics (Springer, Berlin, 1997), Vol. 34.

[31] A. Veretennikov, in *Modern Problems of Stochastic Analysis and Statistics*, edited by V. Panov (Springer, Cham, 2017), pp. 457–511.

[32] J.-F. Delmas and B. Jourdain, Does waste recycling really improve the multi-proposal Metropolis–Hastings algorithm? An analysis based on control variates, J. Appl. Probab. **46**, 938 (2009).

[33] M. Athènes, Conditioning and enhanced sampling schemes for simulating thermodynamic and kinetic properties of condensed matter, Habilitation à diriger des recherches, Université Paris Saclay, Université Paris Sud, 2018, https://hal-cea.archives-ouvertes.fr/tel-01851686.

[34] D. Frenkel, Speed-up of monte carlo simulations by sampling of rejected states, Proc. Natl. Acad. Sci. USA **101**, 17571 (2004).

[35] D. Frenkel, *Waste-Recycling Monte Carlo* (Springer, Berlin, 2006), pp. 127–137.

[36] M. Athènes, Web ensemble averages for retrieving relevant information from rejected monte carlo moves, Eur. Phys. J. B **58**, 83 (2007).

[37] M. Athènes and M.-C. Marinica, Free energy reconstruction from steered dynamics without post-processing, J. Comput. Phys. **229**, 7129 (2010).

[38] G. Adjanor, M. Athènes, and J. Rodgers, Waste-recycling monte carlo with optimal estimates: Application to free energy calculations in alloys, J. Chem. Phys. **135**, 044127 (2011).

[39] L. Cao, G. Stoltz, T. Lelièvre, M.-C. Marinica, and M. Athènes, Free energy calculations from adaptive molecular dynamics simulations with adiabatic reweighting, J. Chem. Phys. **140**, 104108 (2014).

[40] M. Athènes and P. Terrier, Estimating thermodynamic expectations and free energies in expanded ensemble simulations: Systematic variance reduction through conditioning, J. Chem. Phys. **146**, 194101 (2017).

[41] D. Frenkel, K. J. Schrenk, and S. Martiniani, Monte carlo sampling for stochastic weight functions, Proc. Natl. Acad. Sci. USA **114**, 6924 (2017).

[42] See Supplemental Material at http://link.aps.org/supplemental/10.1103/PhysRevMaterials.6.013805 for a detailed derivation of the bridging law from the law of total covariance in Sec. I, results of conventional kMC simulations with moderate dynamical trapping in Sec. II, analysis of the algebraic decay of the transient regime towards the asymptotic diffusion regime in Sec III.

[43] R. E. Caflisch, Monte Carlo and quasi-Monte Carlo methods, Acta Numer. **7**, 1 (1998).

[44] M. Athènes, P. Bellon, and G. Martin, Identification of novel diffusion cycles in B2 ordered phases by Monte Carlo simulation, Philos. Mag. A **76**, 565 (1997).

[45] B. Puchala, M. L. Falk, and K. Garikipati, An energy basin finding algorithm for kinetic Monte Carlo acceleration, J. Chem. Phys. **132**, 134104 (2010).

[46] M. Athènes and V. V. Bulatov, Path Factorization Approach to Stochastic Simulations, Phys. Rev. Lett. **113**, 230601 (2014).

[47] M. Athènes, S. Kaur, G. Adjanor, T. Vanacker, and T. Jourdan, Elastodiffusion and cluster mobilities using kinetic monte carlo simulations: Fast first-passage algorithms for reversible diffusion processes, Phys. Rev. Materials **3**, 103802 (2019).

[48] D. J. Sharpe and D. J. Wales, Efficient and exact sampling of transition path ensembles on Markovian networks, J. Chem. Phys. **153**, 024121 (2020).

[49] D. J. Wales, Calculating rate constants and committor probabilities for transition networks by graph transformation, J. Chem. Phys. **130**, 204111 (2009).

[50] M. A. Novotny, Monte Carlo Algorithms with Absorbing Markov Chains: Fast Local Algorithms for Slow Dynamics, Phys. Rev. Lett. **74**, 1 (1995).

[51] T. Opplestrup, V. V. Bulatov, G. H. Gilmer, M. H. Kalos, and B. Sadigh, First-Passage Monte Carlo Algorithm: Diffusion without All the Hops, Phys. Rev. Lett. **97**, 230602 (2006).

[52] T. Oppelstrup, V. V. Bulatov, A. Donev, M. H. Kalos, G. H. Gilmer, and B. Sadigh, First-passage kinetic Monte Carlo method, Phys. Rev. E **80**, 066701 (2009).

[53] A. Donev, V. V. Bulatov, T. Oppelstrup, G. H. Gilmer, B. Sadigh, and M. H. Kalos, A First-Passage Kinetic Monte Carlo algorithm for complex diffusion-reaction systems, J. Comput. Phys. **229**, 3214 (2010).

[54] G. Nandipati, Y. Shim, and J. G. Amar, First-passage time approach to kinetic monte carlo simulations of metal (100) growth, Phys. Rev. B **81**, 235415 (2010).

[55] K. A. Fichthorn and Y. Lin, A local superbasin kinetic monte carlo method, J. Chem. Phys. **138**, 164104 (2013).

[56] A. Chatterjee and A. F. Voter, Accurate acceleration of kinetic Monte Carlo simulations through the modification of rate constants, J. Chem. Phys. **132**, 194101 (2010).

[57] V. Barbe and M. Nastar, A self-consistent mean field calculation of the phenomenological coefficients in a multicomponent alloy with high jump frequency ratios, Philos. Mag. **86**, 1513 (2006).

[58] H. Rust, Spectral analysis for stochastic processes (2007), lecture notes for the E2C2 / GIACS Summer School, Comorova, Romania.

[59] J. Settino, N. W. Talarico, F. Cosco, F. Plastina, S. Maniscalco, and N. Lo Gullo, Emergence of anomalous dynamics from the underlying singular continuous spectrum in interacting many-body systems, Phys. Rev. B **101**, 144303 (2020).

[60] R. M. Ziff, Spanning Probability in 2D Percolation, Phys. Rev. Lett. **69**, 2670 (1992).

[61] K.-Y. Tsai, M.-H. Tsai, and J.-W. Yeh, Sluggish diffusion in Co-Cr-Fe-Mn-Ni high-entropy alloys, Acta Mater. **61**, 4887 (2013).

[62] A. Paul, Comments on "Sluggish diffusion in Co-Cr-Fe-Mn-Ni high-entropy alloys" by K.Y. Tsai, M.H. Tsai and J.W. Yeh, Acta Mater. **61**, 4887 (2013) Scr. Mater. **135**, 153 (2017).

[63] D. Miracle and O. Senkov, A critical review of high entropy alloys and related concepts, Acta Mater. **122**, 448 (2017).

[64] Y. N. Osetsky, L. K. Béland, A. V. Barashev, and Y. Zhang, On the existence and origin of sluggish diffusion in chemically disordered concentrated alloys, Curr. Opin. Solid State Mater. Sci. **22**, 65 (2018).

[65] J. Kottke, D. Utt, M. Laurent-Brocq, A. Fareed, D. Gaertner, L. Perrière, Ł. Rogal, A. Stukowski, K. Albe, S. V. Divinski *et al.*, Experimental and theoretical study of tracer diffusion in a series of $(CoCrFeMn)_{100-x}Ni_x$ alloys, Acta Mater. **194**, 236 (2020).

[66] M. S. Daw and M. Chandross, Sluggish diffusion in random equimolar fcc alloys, Phys. Rev. Materials **5**, 043603 (2021).

[67] C. Lapointe, T. D. Swinburne, L. Thiry, S. Mallat, L. Proville, C. S. Becquart, and M.-C. Marinica, Machine learning surrogate models for prediction of point defect vibrational entropy, Phys. Rev. Materials **4**, 063802 (2020).

[68] W. Li and Y. Ando, Effect of local structural disorder on lithium diffusion behavior in amorphous silicon, Phys. Rev. Materials **4**, 045602 (2020).

[69] M. Grabowski, J. Rogal, and R. Drautz, Kinetic Monte Carlo simulations of vacancy diffusion in nondilute Ni-X (X = Re, W, Ta) alloys, Phys. Rev. Materials **2**, 123403 (2018).

[70] M. Landeiro Dos Reis, L. Proville, M.-C. Marinica, and M. Sauzay, Atomic scale simulations for the diffusion-assisted crossing of dislocation anchored by vacancy clusters, Phys. Rev. Materials **4**, 103603 (2020).

[71] M. M. Rahman, F. El-Mellouhi, O. Bouhali, C. S. Becquart, and N. Mousseau, Pressure effect on diffusion of carbon at the $85.91^\circ\langle 100\rangle$ symmetric tilt grain boundary of α-iron, Phys. Rev. Materials **5**, 043605 (2021).